




Extensive study of the optical, mechanical properties, and gamma photon shielding effectiveness of potassium titanate biso-phosphate glasses

Y. S. Rammah^{1,*} , F. I. El-Agawany¹, E. Haily², L. Bih^{2,3}, E. M. Ahmed⁴, and K. A. Mahmoud^{5,6}

¹Department of Physics, Faculty of Science, Menoufia University, Shebin El-Koom 32511, Egypt

²Equipe Physico-Chimie La Matière Condensée (PCMC), Faculté Des Sciences de Meknès, Meknès, Morocco

³Laboratoire Des Sciences Et Métiers de L'Ingénieur (LSMI), Département Matériaux Et Procédés, ENSAM Meknès, Université Moulay Ismail, Meknès, Morocco

⁴Department of Physics, College of Science, Taif University, P.O. Box 11099, Taif 21944, Saudi Arabia

⁵Ural Federal University, St. Mira, 19, 620002 Yekaterinburg, Russia

⁶Nuclear Materials Authority, Maadi, Cairo, Egypt

Received: 14 April 2021

Accepted: 7 June 2021

Published online:

23 June 2021

© The Author(s), under exclusive licence to Springer Science+Business Media, LLC, part of Springer Nature 2021

ABSTRACT

This work presents an extensive study of the optical (linear/non-linear), mechanical properties and gamma-photon-shielding effectiveness of potassium titanate biso-phosphate with chemical form $50\text{P}_2\text{O}_5\text{-}30\text{TiO}_2\text{-}(20\text{-}x)\text{K}_2\text{O-xBi}_2\text{O}_3$: $x = 0$ (Bi-0) mol%, 5 (Bi-5) mol%, 10 (Bi-10) mol%, 15 (Bi-15) mol%, and 20 (Bi-20) mol%. The linear refractive index (n^{optical}) increased from 2.41 for Bi-0 sample to 2.52 for Bi-20 sample. Both optical susceptibility ($\chi^{(3)}$) and non-linear refractive index (n_2^{optical}) were enhanced with the addition of Bi^{3+} ions in the investigated glasses. Bond compression bulk elastic (K_{B-C}) modulus was found to decrease from 72.737 GPa for Bi-0 to 69.266 GPa for Bi-20 glasses, while Poisson's ratio (σ_{B-C}) for Bi-glasses was increased from 0.251 to 0.256. According to Makishima-Mackenzie (M-M) model, values of (K_{M-M}) were decreased from 39.370 GPa to 36.775 GPa. In terms of mass and linear attenuation coefficients (MAC and LAC), the glasses take the order that $(\text{Bi-0})^{\text{MAC,LAC}} < (\text{Bi-5})^{\text{MAC,LAC}} < (\text{Bi-10})^{\text{MAC,LAC}} < (\text{Bi-15})^{\text{MAC,LAC}} < (\text{Bi-20})^{\text{MAC,LAC}}$. In terms of half value layer (HVL), at 0.015 MeV, HVL decreased from 0.022 cm to 0.003 cm, while at 15 MeV, it decreased from 12.062 cm to 4.841 cm for Bi-0 and Bi-20 glasses. In terms of transmission factor (TF), the average photons absorbed in the energy interval between 0.15 MeV and 1.5 MeV is 43.34%, 51.60%, 57.59%, 62.02%, and 65.16% of the incoming photons for glasses Bi-0, Bi-5, Bi-10, Bi-15, and Bi-20, respectively. The calculated values of exposure and energy absorption buildup factors (EBF and EABF) increase with increasing the penetration depth (PD) values, and a high increase is detected for high PD values (i.e.,

Address correspondence to E-mail: dr_yasser1974@yahoo.com

PD > 20 mfp). The fast neutron removal cross-section (Σ_R) takes values 0.03248 cm²/g, 0.02931 cm²/g, 0.02691 cm²/g, 0.02504 cm²/g, and 0.02355 cm²/g for glass samples Bi-0, Bi-5, Bi-10, Bi-15, and Bi-20, respectively.

1 Introduction

Currently, phosphate-based glasses are applied in different areas due to their unique advantages over other glasses such as germanate, silicate, and borate glasses. Some of these properties such as high-thermal expansion factor, low-melting temperature point, ultraviolet (UV) transmission, high refractive index [1–5]. In other side, phosphate-based glasses have some disadvantages such as poor chemical durability, high hygroscopic, and volatile nature, these make phosphate glasses restrict in their applications [6, 7]. Therefore, several researchers have been aimed to solve these problems in P₂O₅ glasses to make them more stable by introducing oxides such as TiO₂, ZnO, Bi₂O₃, Al₂O₃, CdO, Li₂O, PbO in the glass network [8]. Currently, glasses, semiconductor, and thin films materials have been applied in several electronic and optical applications [9–14].

Introducing bismuth and potassium oxides (Bi³⁺ ions and K₂O) in the phosphate glasses leads to enhance the physical and chemical features of the produced glasses. Shaim et al., and Elmoudane et al., [15, 16] have been studied the impact of Bi³⁺ on structural, thermal, dc conductivity, and dielectric properties of phosphate glasses. Shams et al., [4] studied the structure, dielectric, and gamma-ray efficiency of P₂O₅ glasses. Rao et al., [17] have been investigated the optical properties of phosphate glasses doped with TiO₂. The obtained results of the former studies claimed that the addition of Bi³⁺ ions to P₂O₅ glasses polymerized the vitreous network and induced the creation of water-resist Bi-O-Bi and P-O-Bi linkages. Another observation that the Bi³⁺ ions in phosphate glasses played a dual structural role in the glassy network, either a glass former with [BiO₃] units or a modifier with [BiO₆] octahedral [18]. Moreover, the electrical conductivity reduced, while the real permittivity enhanced with increasing Bi³⁺ ions due to the presence of strong polarizing cations Bi³⁺ ions in the glasses [7]. Indeed, the addition of Bi₂O₃ to TiO₂-P₂O₅ glasses increased the infrared transmission range and enhanced the refractive index of the produced glasses [19]. The produced glasses

also exhibited nonlinear polarizability [17], which made them interesting for optical applications. It was observed that the addition of alkaline oxides such as K₂O to the phosphate system can extend the vitrification region and reduces the melting temperature and increases the glass stability [20].

The current work aimed to investigate the effect of the substitution of potassium (K₂O) by bismuth (Bi₂O₃) on the optical (linear/non-linear), mechanical properties, and gamma-ray shielding effectiveness of biso-phosphate (Bi₂O₃-K₂O-TiO₂-P₂O₅) glasses using MCNP-5 simulation and Phy-X/PSD software to apply these glasses in various optical and medical applications.

2 Materials and methods

2.1 Bi0-Bi20 glasses

Five samples of potassium titanate biso-phosphate glasses with chemical form 50P₂O₅-30TiO₂-(20-x)K₂O-xBi₂O₃: x = 0 mol%, 5 mol%, 10 mol%, 15 mol%, and 20 mol% were chosen from Ref. [21]. These glass samples were synthesized using the reagents K₂CO₃ (Aldrich, 99.6%), Bi₂O₃ (Alfa Aesar, 99.99%), NH₄H₂PO₄ (Aldrich, 99%), and TiO₂ (Aldrich, 99.9%) as precursors to prepare batches of 8 g glass sample via the conventional melt quenching technique. Chemical amounts for each sample were weighed and mixed in a silica mortar for 30 min. The mixture was transferred to an alumina crucible and placed in an electric furnace at 300 °C for 6 h to remove H₂O and NH₃, then at 600 °C for 12 h to decarbonate the compositions, and then the at 1200 °C for 1 h to get the molten glass. Subsequently, the mixture was quenched rapidly at room temperature on a stainless-steel cylindrical shape and pressed to form glass pellets [21]. The studied samples are denoted by the following keys:

Bi-0: 50P₂O₅ – 30TiO₂ – 20K₂O – 0Bi₂O₃,

Bi-5: 50P₂O₅ – 30TiO₂ – 15K₂O – 5Bi₂O₃,

Bi-10: 50P₂O₅ – 30TiO₂ – 10K₂O – 10Bi₂O₃,

Bi-15: 50P₂O₅ – 30TiO₂ – 5K₂O – 15Bi₂O₃, and
Bi-20: 50P₂O₅ – 30TiO₂ – 0K₂O – 20Bi₂O₃. Glass keys, chemical composition, density, and molar volume were listed in Table 1.

2.2 Methods

2.2.1 Linear/non-linear optical parameters

For non-crystalline materials, the optical parameters can be evaluated with the help of the following relations [22–27]:

(i) The linear refractive index ($n^{optical}$),

$$\frac{[(n^{optical})^2 - 1]}{[(n^{optical})^2 + 2]} = 1 - \left(\frac{E^{optical}}{20}\right)^{1/2} \tag{1}$$

(ii) Molar refraction (R^{molar}),

$$R^{molar} = \left(\frac{(n^{optical})^2 - 1}{(n^{optical})^2 + 2}\right) V^{molar} \tag{2}$$

(iii) Electronic polarizability (α^{molar}),

$$\alpha^{molar} = \frac{R^{molar}}{2.52} \tag{3}$$

(iv) The optical electronegativity (χ^*)

$$\chi^* = 0.2688E^{optical} \tag{4}$$

(v) Linear dielectric susceptibility ($\chi^{(1)}$)

$$\chi^{(1)} = ((n^{optical})^2 - 1)/4\pi \tag{5}$$

(vi) Optical susceptibility (χ^3)

$$\chi^3(esu) = A/(4\pi)^4(n^{optical} - 1)^4 \tag{6}$$

(vii) Non-linear refractive index ($n_2^{optical}$)

$$n_2^{optical}(esu) = \frac{12\pi\chi^3}{n^{linear}} \tag{7}$$

Here, $E^{optical}$ and V^{molar} are the optical energy gap and the molar volume of the material. $A = 1.7 \times 10^{-10}$ is a constant obtained by fitting the experimental values of n^{linear} and $\chi^{(3)}$ of different oxides.

2.2.2 Mechanical properties

In this work, the mechanical factors including (Young’s, bulk, longitudinal, and shear) elastic moduli and Poisson’s ratio of the studied Bi-glasses were calculated via two methods: (i) bond compression (B-C) model and (ii) Makishima-Mackenzie (M-M) model. Procedures and relations of calculations were applied as in earlier reports [28–30] as well as in Tables 2 and 3.

2.2.3 MCNP-5 simulation and Phy-X/PSD software

The elemental chemical compositions and densities presented in Table 1 were used by the Monte Carlo simulation code MCNP-5 and Phy-X/PSD program to estimate the studied glasses’ radiation shielding properties. Based on the nuclear database’s primary sources ENDF, ACTI, ENDL, ACTI, and T-16 files, the mean track length (MTL) of gamma photons was simulated [31]. A geometry also describes the

Table 1 Key, chemical composition, density, molar volume, and energy gap of 50P₂O₅-30TiO₂-(20-x)K₂O-xBi₂O₃-: (x = 0, 5, 10, 15, and 20 mol%)

Sample key	Composition, (mol%)				Density, ρ (g/cm ³) \pm 0.02	Vm (cm ³ /mol) \pm 0.03	Energy gap, $E^{optical}$ (eV) 0.01
	P ₂ O ₅	TiO ₂	K ₂ O	Bi ₂ O ₃			
Bi-0	50	30	20	0	2.58	44.03	2.95
Bi-5	50	30	15	5	2.93	45.05	2.91
Bi-10	50	30	10	10	3.27	46.08	2.83
Bi-15	50	30	5	15	3.58	47.33	2.75
Bi-20	50	30	0	20	3.84	48.86	2.56

Table 2 The values of total number of cationic per glass formula unit (η), average cross-link density (\bar{n}_c), average stretching force constant (\bar{F}), number of network bond per unit volume (n_b), average bond length (l), calculated bond compression elastic moduli (bulk (K_{B-C}), shear (S_{B-C}), longitudinal (L_{B-C}), Young's (E_{B-C}) and Poisson's ratio (σ_{B-C}) of Bi-glasses. x_i : molar fraction of the i^{th} constituent, n_c : the number of crosslinks for each cation of the oxide, and N_C : the number of cations per unit glass formula

Parameters and elastic moduli	Bi-0	Bi-5	Bi-10	Bi-15	Bi-20
η	1.7	1.7	1.7	1.7	1.7
$\bar{n}_c = \frac{1}{\eta} \sum x_i (n_c)_i (N_C)_i$	1.529	1.500	1.470	1.441	1.411
$\bar{F} = \frac{\sum (x n_f)_i (N/m)}{\sum (x n_f)_i}$	312.608	315.956	319.377	322.876	326.454
$n_b = \frac{N_A}{V_m} \sum (n_f x)_i \times 10^{28} (m^{-3})$	6.391	6.082	5.880	5.661	5.423
$l = \left(0.0106 \frac{\bar{F}}{K_{B-C}}\right)^{0.26} (nm)$	0.447	0.450	0.452	0.455	0.458
$K_{B-C} = \frac{N_A}{9V_m} \sum_i (n_f x \bar{F}^2) (GPa)$	72.737	72.099	71.474	70.546	69.266
$S_{B-C} = \left(\frac{3}{2}\right) K_{B-C} \left(\frac{1-2\sigma_{B-C}}{1+\sigma_{B-C}}\right) (GPa)$	43.269	42.636	42.009	41.204	40.196
$L_{B-C} = K_{B-C} + \frac{4}{3} S_{B-C} (GPa)$	130.285	128.806	127.347	125.348	122.727
$E_{B-C} = 2S_{B-C} (1 + \sigma_{B-C}) (GPa)$	108.327	106.848	105.382	103.469	101.403
$\sigma_{B-C} = 0.28 (\bar{n}_c)^{-0.25}$	0.251	0.253	0.254	0.255	0.256

Table 3 Total ionic packing density (V_t), total dissociation energy (G_t), Young's modulus (E_{M-M}), bulk modulus (K_{M-M}), shear modulus (S_{M-M}), and Poisson's ratio (σ_{M-M}) based on Makishima-Mackenzie model of Bi-glasses

Parameters and elastic moduli	Bi-0	Bi-5	Bi-10	Bi-15	Bi-20
$V_t = \left(\frac{1}{V_m}\right) \sum_i (V_i x_i)$	0.582	0.576	0.569	0.560	0.549
$G_t = \sum_i (G_i x_i) (KJ/m^3)$	48.3	48.92	49.54	50.16	50.78
$E_{M-M} = 2V_t G_t (GPa)$	56.296	56.389	56.442	56.264	55.789
$K_{M-M} = 1.2V_t E_{M-M} (GPa)$	39.370	38.971	38.583	37.867	36.775
$S_{M-M} = (3E_{M-M} K_{M-M}) / (9K_{M-M} - E_{M-M}) (GPa)$	22.310	22.387	22.465	22.463	22.366
$\sigma_{M-M} = \left(\frac{E_{M-M}}{2G_{M-M}}\right) - 1 (GPa)$	0.261	0.258	0.256	0.252	0.247

problem components cell, surface, source, material, and cut of cards should arrange. The 3D representation for the geometry used to simulate the present

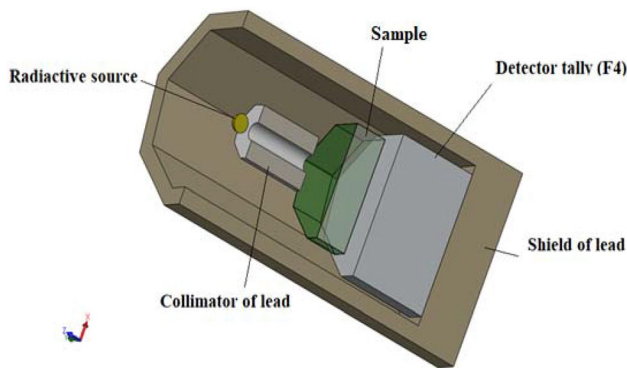


Fig. 1 The 3D representation for the geometry used to simulate the shielding parameters of Bi-glasses

study's shielding parameters is illustrated in Fig. 1. Figure 1 depicts a radioactive gamma-ray source placed in the center of the geometry. It emits energies varied in the range between 0.015 MeV and 15 MeV along the positive Z-axis. The photon flux emitted by the radioactive source was collimated using a collimator of lead. The glass -photons interaction takes place after the collimated photons were directed to the fabricated samples. Then, transmitted photons were detected by the detector, where the detector was assumed to be an F4 tally to estimate the mean track length (MTL) of incident gamma photons. The cut-off card was set up to stop the interaction after 10^6 particles [32, 33].

The most important radiation protection parameters for materials are as the following with their relations [34–47]:

- (i) Mass and linear attenuation coefficients (MAC and LAC),

$$(MAC)_{sample} = \left(\frac{\mu}{\rho}\right)_{sample} = \sum_i W_i \left(\frac{\mu}{\rho}\right)_i \tag{8}$$

$$(LAC)_{sample} = (\mu)_{sample} = (MAC)_{sample} \times (\rho)_{sample} \tag{9}$$

- (ii) Half value layer (HVL),

$$(HVL)_{sample} = \frac{0.693}{(\mu)_{sample}} \tag{10}$$

- (iii) Mean free path (MFP),

$$(MFP)_{sample} = (\mu^{-1})_{sample} \tag{11}$$

- (iv) Effective atomic number (Z_{eff}),

$$(Z_{eff})_{sample} = \frac{\sum_i f_i A_i \left(\frac{\mu}{\rho}\right)_i}{\sum_j \frac{A_j}{Z_j} \left(\frac{\mu}{\rho}\right)_j} \tag{12}$$

Here, A_i , Z_i , and f_i are the atomic weight, the atomic number, and the fractional abundance of the element i relative to the number of atoms providing that $\sum f_i = 1$.

3 Results and discussion

3.1 Linear/non-linear optical properties

With the help of the indirect optical energy gap ($E^{optical}$) values of the investigated Bi0-Bi20 glasses [21], the corresponding values of refractive index ($n^{optical}$) are calculated via Eq. (1) and listed in Table 4. Figure 2a shows the dependence of ($E^{optical}$) on Bi^{3+} ions in Bi-glasses. The decrease in the ($E^{optical}$) from 2.95 eV (Bi-0) to 2.56 eV (Bi-20) can be explained as the reduction the addition of Bi_2O_3 concentration mol% of the studied glasses results in damage in the network structure of glass system leads to increasing the number of nonbridging oxygen (NBO) atoms. In other words, the decreasing in ($E^{optical}$) with the introduction of Bi^{3+} ions in Bi-glasses can be related to the polarizing effect of Bi_2O_3 and/or the enhancement of the overlapping of the oxygen O2p and bismuth 6 s and 6p orbitals in the band gap [3, 21]. Figure 2b depicts the dependence of the refractive index ($n^{optical}$) on Bi^{3+} in Bi-glasses. It is found that the ($n^{optical}$) increased from 2.41 for Bi-0 glass sample to 2.52 for Bi-20 glass sample.

Figure 3a and b depict the dependence of the (R^{molar}) and (α^{molar}) on Bi^{3+} ions content in the studied Bi0-Bi20 samples. It is noticed that the values of (R^{molar}) are in a direct behavior with the values of (α^{molar}). The increase in both (R^{molar}) and (α^{molar}) with the addition of Bi^{3+} ions content in Bi-glasses relates to the increasing of the number of nonbridging oxygen (NBO) atoms in the glass structure. This may be attributed to the increment of the molar volume (V_m) of the glass samples with increasing Bi_2O_3 (from 44.03 cm^3/mol for Bi-0 glass sample to 48.86

Table 4 $E^{optical}$, R^{molar} , α^{molar} , R^{loss} , $T^{optical}$, $M^{criterion}$, ϵ^{static} , $\epsilon^{optical}$, $M(n)$, $M(E^{optical})$, (χ^*), ($\chi^{(1)}$), (χ^3), and ($n_2^{optical}$) of the studied glasses

Physical parameter	Sample key				
	Bi-0	Bi-5	Bi-10	Bi-15	Bi-20
Linear refractive index, $n^{optical} \pm 0.01$ P.W*	2.41	2.42	2.44	2.46	2.52
Molar refractivity, R^{molar} (cm^3/mol) ± 0.001 P.W*	31.101	31.925	32.867	33.979	35.628
Molar polarizability, $\alpha^{molar} \times 10^{-24} cm^3 \pm 0.001$ P.W*	12.341	12.668	13.042	13.483	14.138
Optical electronegativity (χ^*) ± 0.001 P.W*	0.792	0.782	0.760	0.739	0.688
Linear electric/dielectric susceptibility ($\chi^{(1)}$) ± 0.001 P.W*	0.383	0.387	0.396	0.405	0.428
Non-linear optical susceptibility (χ^3) $\times 10^{-12}$ (esu) ± 0.001 P.W*	3.660	3.826	4.185	4.586	5.745
Non-linear refractive index ($n_2^{optical}$) $\times 10^{-10}$ (esu) ± 0.001 P.W*	5.721	5.953	6.451	7.003	8.567

P.W* = Present work

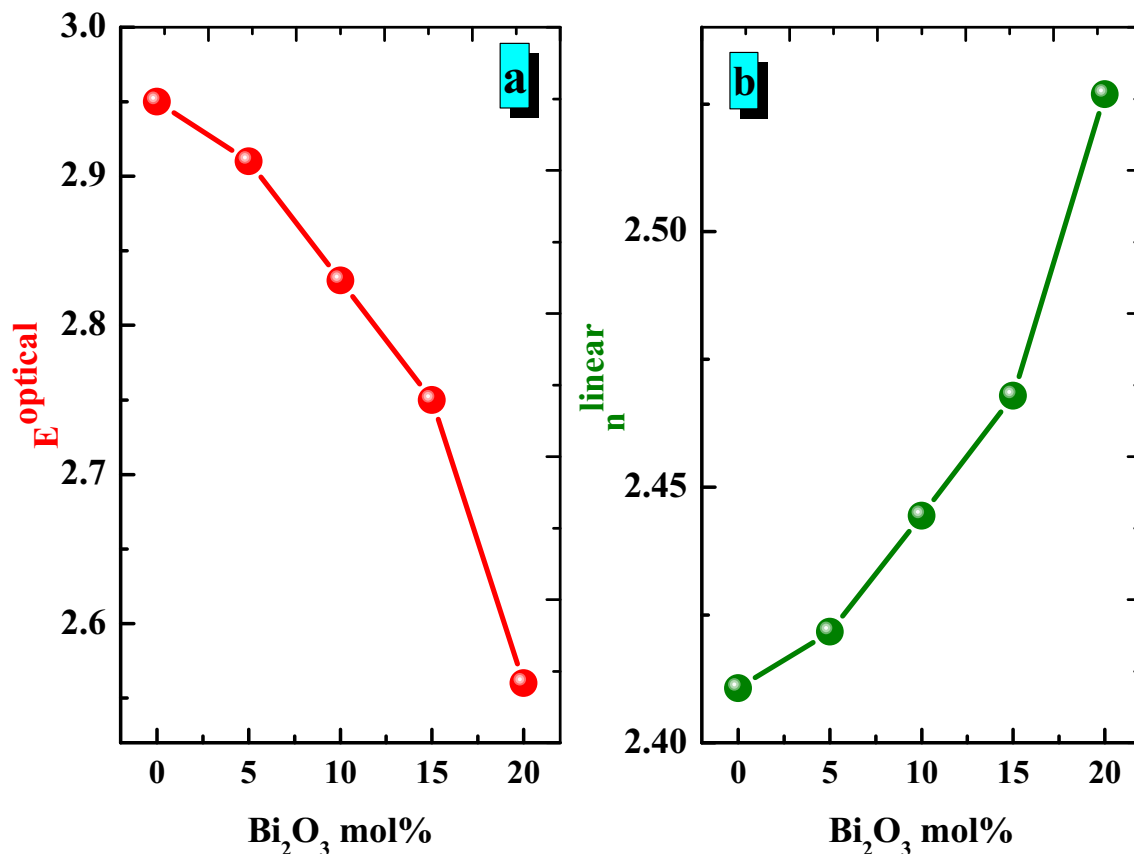


Fig. 2 Dependence of **a** E^{optical} and **b** n^{optical} on Bi_2O_3 concentration mol% of $50\text{P}_2\text{O}_5\text{-}30\text{TiO}_2\text{-(}20\text{-x)K}_2\text{O-xBi}_2\text{O}_3$: $x = 0, 5, 10, 15,$ and 20 mol% (Bi0-Bi-20) glasses

cm^3/mol for Bi-20 glass sample). The increasing trend of molar volume (V_m) trend can be attributed to larger molar volume of $\text{Bi}_2\text{O}_3 = 52.35 \text{ cm}^3/\text{mol}$ than that of $\text{K}_2\text{O} = 40.08 \text{ cm}^3/\text{mol}$. Thus, the addition of Bi^{3+} content leads to the opening of the glassy structure by raising the bond length and thereafter the interatomic spacing. The increase of the NBO in the glassy structure will support the connection of structural units by sharing their corners and the interaction between Bi_2O_3 (BiO_6) and P_2O_5 (PO_4) and form P-O-Bi bonds [21]. The obtained values of (R^{molar}) and (α^{molar}) are listed in Table 4.

Figure 4a depicts the dependence of the optical electronegativity (χ^*) on Bi^{3+} ions in Bi-glasses, while Fig. 4b shows the dependence of the linear dielectric/dielectric susceptibility $\chi^{(1)}$. As shown in Fig. 3 and Table 4, the value of χ^* reduces from 0.792 to 0.688, while $\chi^{(1)}$ increases from 0.383 to 0.428 with the increase of Bi^{3+} ions from 0 mol% to 20 mol%. These trends attributed to the defects that occurred in the glass network after introducing the Bi^{3+} ions and the

increasing number of nonbridging oxygen (NBO) atoms in the glass framework.

Figure 5a and b illustrate the variation of the $\chi^{(3)}$ and n_2^{optical} with Bi^{3+} ions content in the studied Bi-glasses. Values of the $\chi^{(3)}$ and n_2^{optical} are listed in Table 4. Both of the $\chi^{(3)}$ and n_2^{optical} enhances with the addition of Bi^{3+} ions in the investigated glasses, this may be due to the increase in the number non-bridging oxygen (NBO) number in glass structures, which simplify the connection of structural units by sharing their corners and the interaction between Bi_2O_3 (BiO_6) and P_2O_5 (PO_4) and create P-O-Bi bonds [3].

3.2 Mechanical properties

Applying the bond compression (B-C) model in order to evaluate the mechanical properties of the investigated Bi-glasses, the required physical parameters and their values are tabulated in Table 2. Figure 6 depicts the variation of bond compression elastic

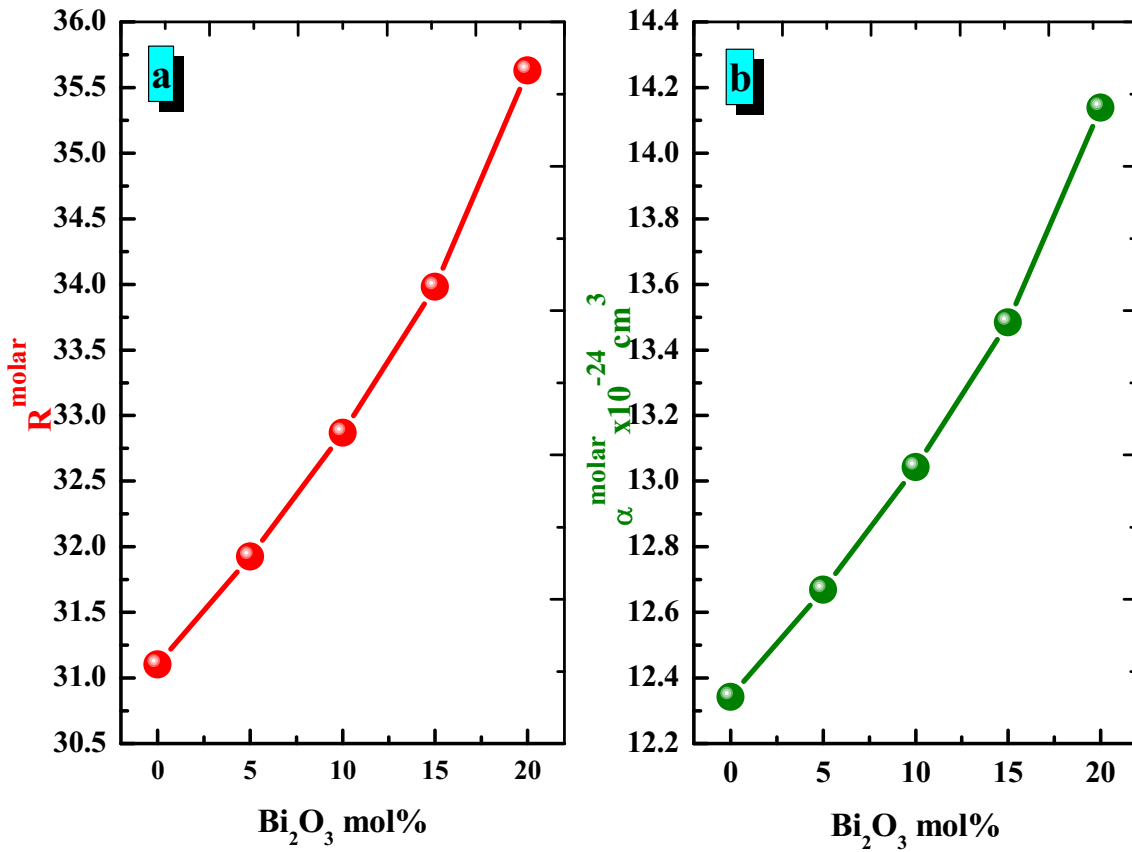


Fig. 3 Dependence of a R^{molar} and b α^{molar} on Bi_2O_3 concentration mol% of Bi0-Bi-20 glasses

moduli (Young’s (E_{B-C}), bulk (K_{B-C}), longitudinal (L_{B-C}), and shear (S_{B-C})) with Bi^{3+} ions content in Bi-glasses. It is found that there is a decrement in all modulus of elasticity, this trend may be due to the substitution of Bi_2O_3 with a coordination number equal to 3 by K_2O with coordination number of 4. This change in the glass network leads to the decrement of total number of bonds. Values of bulk elastic (K_{B-C}) modulus were found to decrease from 72.737 GPa for Bi-0 (glass sample free with Bi_2O_3) to 69.266 GPa for Bi-20 (glass sample rich with Bi_2O_3). This decrease in (K_{B-C}) can be attributed to both the number of the network bonds per unit volume (n_b) and the average bond lengths (l) which depends on the first order stretching-force constant (\bar{F}) [28–30]. The addition of Bi^{3+} ions leads the (n_b) to decrease from 6.391 to $5.423 \times 10^{28} \text{ (m}^{-3}\text{)}$ despite of the increasing the (\bar{F}) from 312.608 to 326.454 (N/m). Indeed, the average crosslink density (\bar{n}_c) decreases from 1.517 to 1.411 due to the lower coordination number of Bi_2O_3 . Bond compression values of Young’s (E_{B-C}) elastic modulus were found to

decrease from 108.327 GPa to 101.403 GPa, from 43.269 GPa to 40.196 GPa for shear (S_{B-C}), and from 130.285 GPa to 122.727 GPa for longitudinal (L_{B-C}). Due to the decrease of the (\bar{n}_c), values of Poisson’s ratio (σ_{B-C}) for Bi-glasses were increased from 0.251 to 0.256.

In this work, moduli of elasticity of the investigated Bi-glasses were evaluated based on the Makishima and Mackenzie (M-M) model [28–30]. The physical quantities required to apply this model are tabulated in Table 5. Figure 7 shows the variation of packing density and dissociation energy with Bi^{3+} ions content of Bi0-Bi-20 glasses. From this figure, the addition of B_2O_3 will decrease the packing density (V_t) from 0.582 to 0.549. On the contrary, the dissociation energy (G_t) increases from 48.3 kJ/m^3 to 50.78 kJ/m^3 . The increase in the (G_t) for Bi-glasses attributed to the dissociation energy per unit volume of Bi_2O_3 (31.6 kJ/m^3) is higher than that of K_2O (19.2 kJ/m^3). The obtained data of (M-M) elastic moduli (Young’s (E_{M-M}), bulk (K_{M-M}), and shear (S_{M-M})) and Poisson’s ratio (σ_{M-M}) are listed in Table 3 and illustrated in

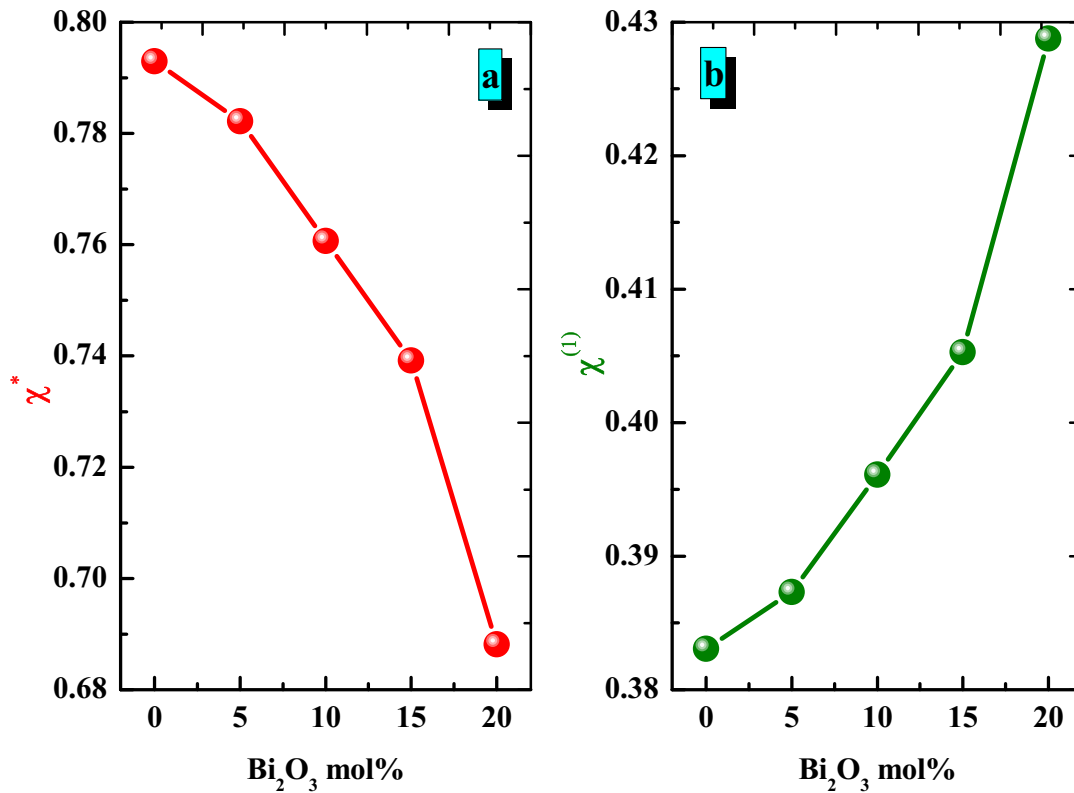


Fig. 4 Dependence of χ^* and $\chi^{(1)}$ on Bi_2O_3 concentration mol% of Bi0-Bi-20 glasses

Fig. 8. Therefore, the substitution of Bi_2O_3 by K_2O leads to a slight decrease of values of (E_{M-M}) from 56.296 GPa to 55.789 GPa, (K_{M-M}) from 39.370 GPa to 36.775 GPa, and slight increases in the (S_{M-M}) from 22.310 to 22.366 (GPa). Poisson's ratio (σ_{M-M}) for Bi-glasses was decreased from 0.261 to 0.247. The trend of all elastic moduli is in good agreement with that in B-C model.

3.3 Gamma-ray shielding effectiveness

In this study, the gamma-ray shielding efficacies of heavy metal oxide glasses (HMO) based on bismuth Bi_2O_3 followed by the chemical formula $50\text{P}_2\text{O}_5-30\text{TiO}_2-(20-x) \text{K}_2\text{O}-x\text{Bi}_2\text{O}_3$ -: ($x = 0 \text{ mol}\%$, $5 \text{ mol}\%$, $10 \text{ mol}\%$, $15 \text{ mol}\%$, $20 \text{ mol}\%$) have been investigated. MCNP-5 Monte Carlo code and Phy-X/ PSD [47] online program was used to investigate the effectiveness of the prepared glasses in terms of mass attenuation coefficient (MAC), half-value layer (HVL), mean free path (MFP), effective and equivalent atomic numbers (Z_{eff} , Z_{eq}), transmission and buildup factors (TF, BUFs), and fast neutron removal

cross-section (FNRCs). Table 1 introduced the chemical composition, density, and molar volume of the five glasses coded Bi-0, Bi-5, Bi-10, Bi-15, and Bi-20 used in this study. After that, the MAC results are plotted with respect to photon energy in the 0.015–15 MeV range and presented in Fig. 9. As can be seen from Fig. 9, MAC possesses maximum values at low energy photon and sharply decreased with an exponential trend obeying Beer-Lambert law until reaching 0.09053 MeV a distinguished hump is shown due to the k- absorption edge of (Bi, $z = 83$) found in the glass matrix. This hump gradually increased in height with increasing Bi molar ratio while has been disappeared in the Bi-0 sample as this sample is free of Bi. This low energy zone is characterized by Photoelectric (PE) cross-section dominance, and its relationship with photon energy is presented by $(\sigma)E \propto E^{-3.5}$. After that, Compton scattering (CS) cross-section is dominant, and all-glass samples behave in the same manner as its relationship with photon energy is presented by $(\sigma)S \propto E^{-1}$. The input figure in Fig. 9 presents the Compton scattering zone with a slight change in MAC with photon energy. Finally, the

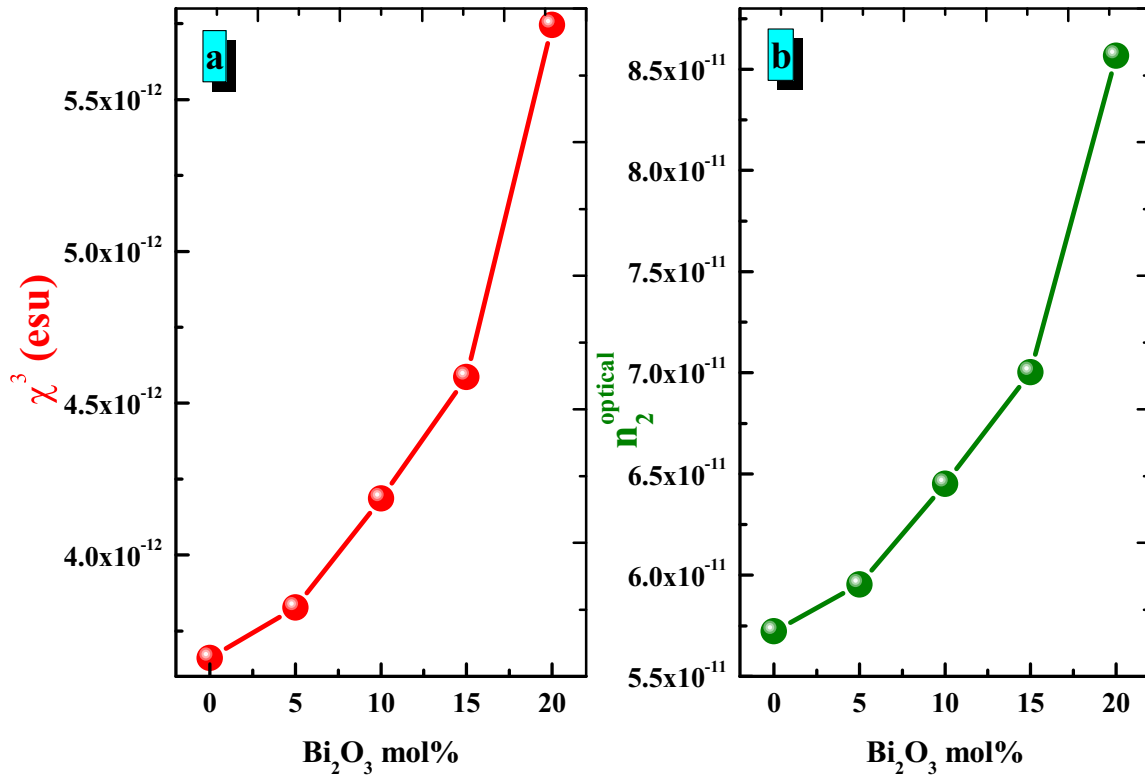


Fig. 5 Dependence of χ^3 and n_2^{optical} on Bi_2O_3 concentration mol% of Bi0-Bi-20 glasses

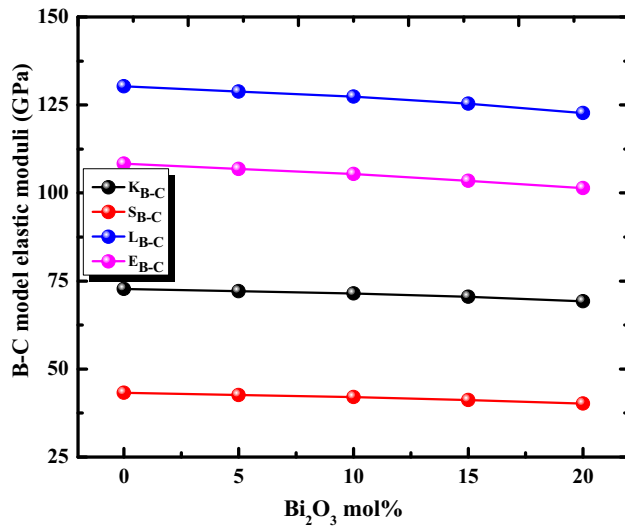


Fig. 6 B-C model elastic moduli of Bi0-Bi-20 glasses

trend that MAC possesses is attributed to the dominance of pair production (PP) as its relationship with photon energy is presented by $(\sigma)P \propto E$. MAC of the prepared Bi glasses obtained from the two methods; MCNP- 5 and Phy-X/PSD, are presented in Table 6, and the relative difference in % between the two methods is calculated from:

$$Dev.(%) = \left| \frac{[(MAC)_{\text{Phy-X/PSD}} - (MAC)_{\text{MCNP}}]}{(MAC)_{\text{Phy-X/PSD}}} \right| \times 100\% \quad (13)$$

and found ranged from -0.003 to 0.0777 , from -0.0259 to 0.2223 , from -0.0413 to 3.0054 , from -0.0450 to 1.4549 , and from -0.0512 to 4.8413 for Bi-0, Bi-5, Bi-10, Bi-15, and Bi-20, respectively, which assured the accuracy of the two used methods that seem to be compatible with each other. Bi samples' MAC values are ranged from $12.1982 \text{ cm}^2/\text{g}$ to $56.8434 \text{ cm}^2/\text{g}$ in the 0.015 MeV , while found ranged from $0.0222 \text{ cm}^2/\text{g}$ to $0.0373 \text{ cm}^2/\text{g}$ for Bi-0 and Bi-20, respectively. All obtained results reach the conclusion that is enhancing such glasses with heavy metal oxide like Bi_2O_3 with $0.0 \text{ mol } \%$ to $20 \text{ mol } \%$ a great positive effect on the shielding efficacies of these glasses and increases the ability to use these glasses in nuclear protection applications. Based on these MAC results, as well as the glass density which found increased from $2.58 \text{ g}/\text{cm}^3$ to $3.84 \text{ g}/\text{cm}^3$ (see Table 1), one can calculate the other effective shielding parameters, namely linear attenuation coefficient (LAC), which seem to be similar to MAC trend with values greater than MAC as it presented by MAC

Table 5 Coordination number per cation (n_f), crosslink density per cation (n_c), cation–anion bond length (r), Stretching force constant (F), packing density factor (V_i), and dissociation/bond energy per unit volume (G_i) of the oxides P_2O_5 , TiO_2 , K_2O , and Bi_2O_3

Oxide	n_f	n_c	r (nm)	F (N/m)	V_i (m^3/mol)	$G_i \times 10^6$ (KJ/ m^3)
P_2O_5	4	2	0.156	450	34.6	28.2
TiO_2	6	4	0.196	226	14.4	101.2
K_2O	4	2	0.219	164	20.2	19.2
Bi_2O_3	3	1	0.240	216	26.1	31.6

Fig. 7 Packing density and dissociation energy of Bi0-Bi-20 glasses

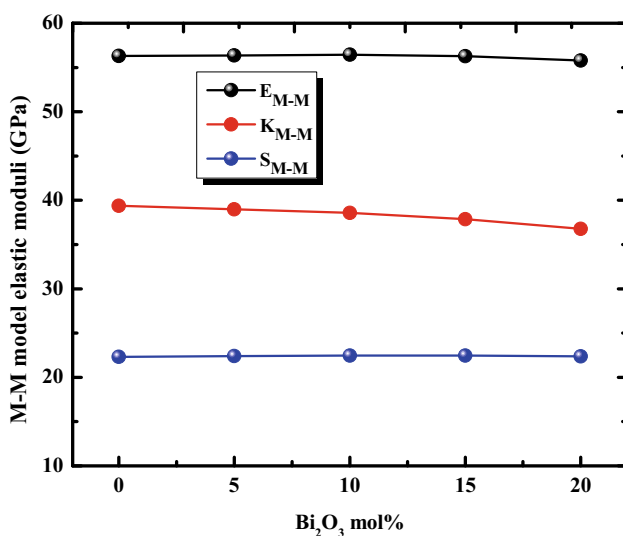
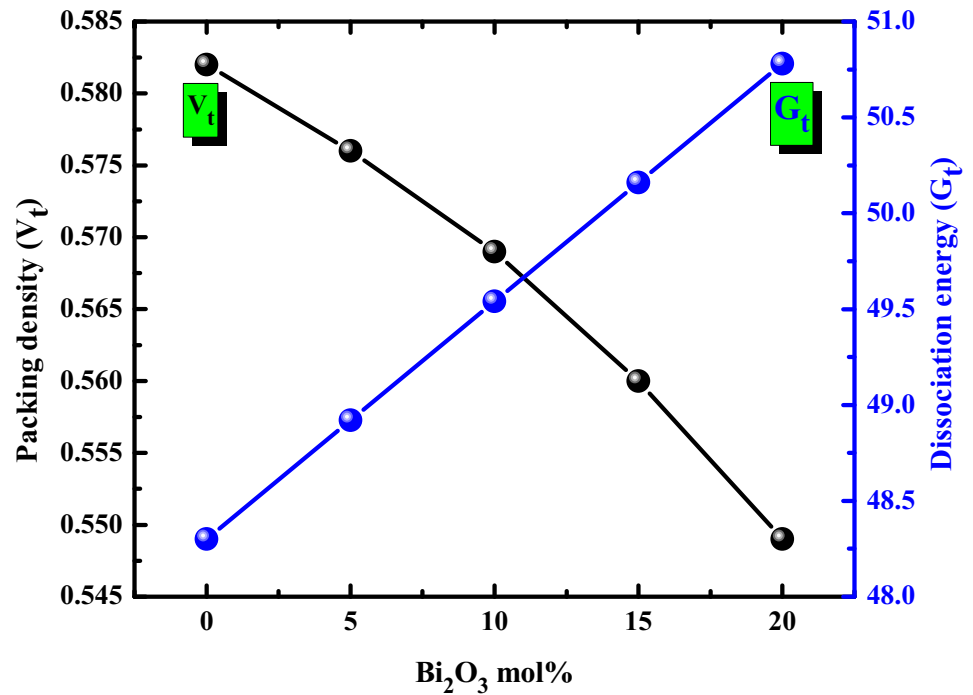


Fig. 8 M-M model elastic moduli of Bi0-Bi-20 glasses

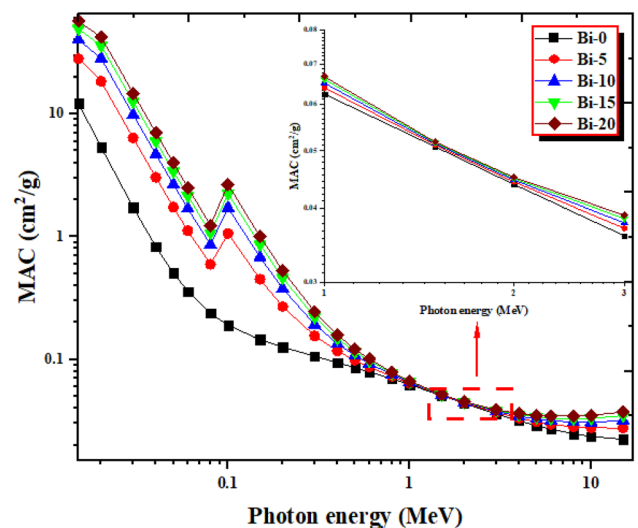


Fig. 9 MAC of Bi0-Bi-20 glasses as a function of photon energy

Table 6 The mass attenuation coefficient simulated using MCNP5 and calculated using the Phy-X/PSD of Bi-glasses

Energy (MeV)	Mass attenuation coefficient (cm ² /g)														
	Bi-0			Bi-5			Bi-10			Bi-15			Bi-20		
	MCNP-5	XCOM	Δ (%)	MCNP-5	XCOM	Δ (%)	MCNP-5	XCOM	Δ (%)	MCNP-5	XCOM	Δ (%)	MCNP-5	XCOM	Δ (%)
0.015	12.1982	12.1925	0.0464	28.0626	28.0721	-0.0339	40.0192	40.0407	-0.0539	49.3550	49.3848	-0.0604	56.8434	56.8824	-0.0686
0.03	1.7356	1.7347	0.0546	6.3691	6.3708	-0.0259	9.8610	9.8651	-0.0413	12.5875	12.5932	-0.0450	14.7746	14.7821	-0.0512
0.05	0.5057	0.5053	0.0777	1.7286	1.7341	-0.3177	2.6502	2.6603	-0.3789	3.3698	3.3834	-0.4033	3.9470	3.9635	-0.4184
0.08	0.2370	0.2370	-0.0003	0.5869	0.5943	-1.2560	0.8506	0.8636	-1.5238	1.0565	1.0738	-1.6404	1.2217	1.2425	-1.7056
0.15	0.1446	0.1447	-0.0899	0.4511	0.4501	0.2223	0.7014	0.6803	3.0054	0.8728	0.8601	1.4549	1.0554	1.0043	4.8413
0.3	0.1062	0.1064	-0.1052	0.1548	0.1553	-0.2812	0.1915	0.1921	-0.3601	0.2211	0.2209	0.0905	0.2440	0.2440	0.0069
0.5	0.0858	0.0858	-0.0801	0.0982	0.0984	-0.2336	0.1076	0.1079	-0.3249	0.1149	0.1154	-0.3869	0.1208	0.1213	-0.4306
0.8	0.0694	0.0694	-0.0929	0.0726	0.0728	-0.2046	0.0751	0.0753	-0.2810	0.0770	0.0772	-0.3395	0.0785	0.0788	-0.3819
1	0.0622	0.0624	-0.3704	0.0633	0.0639	-1.0771	0.0641	0.0651	-1.5925	0.0648	0.0660	-1.9874	0.0653	0.0668	-2.2956
1.5	0.0506	0.0508	-0.3379	0.0508	0.0511	-0.7381	0.0509	0.0514	-1.0384	0.0510	0.0516	-1.2717	0.0510	0.0518	-1.4581
3	0.0358	0.0359	-0.3131	0.0368	0.0370	-0.4409	0.0376	0.0378	-0.5312	0.0382	0.0384	-0.5983	0.0387	0.0389	-0.6516
5	0.0287	0.0288	-0.2542	0.0309	0.0310	-0.2902	0.0326	0.0327	-0.3145	0.0338	0.0340	-0.3318	0.0349	0.0350	-0.3461
8	0.0247	0.0247	-0.2348	0.0281	0.0282	-0.2231	0.0307	0.0308	-0.2208	0.0327	0.0328	-0.2173	0.0344	0.0344	-0.2168
10	0.0235	0.0235	-0.2232	0.0276	0.0276	-0.1978	0.0306	0.0307	-0.1891	0.0330	0.0331	-0.1807	0.0350	0.0350	-0.1766
15	0.0222	0.0223	-0.2220	0.0276	0.0276	-0.1799	0.0316	0.0316	-0.1614	0.0347	0.0348	-0.1466	0.0372	0.0373	-0.1393

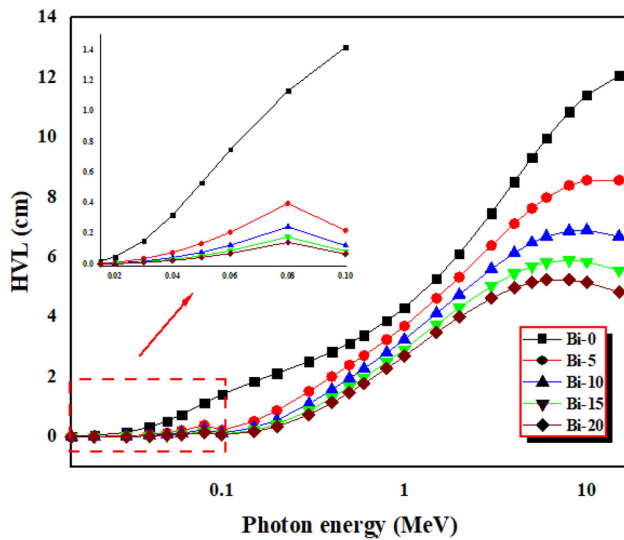


Fig. 10 HVL of Bi0-Bi-20 glasses as a function of photon energy

times the sample density. In terms of MAC and LAC the glasses take the order that Bi-0 < Bi-5 < Bi-10 < Bi-15 < Bi-20. All these discussed parameters introduce the Bi-20 sample as a superior candidate for gamma-ray shielding applications.

Regarding the thickness of glasses used in shielding gamma rays, HVL is an important thickness to be calculated. It is calculated depending on LAC values and varied with an inverse relation with LAC. HVL is presented in Fig. 10 with respect to photon energy for Bi investigated glasses. As expected, HVL is small at a small energy zone and increased with the increase in incident photon energy. The great effect of enhancing these glasses with high molar ratios of Bi

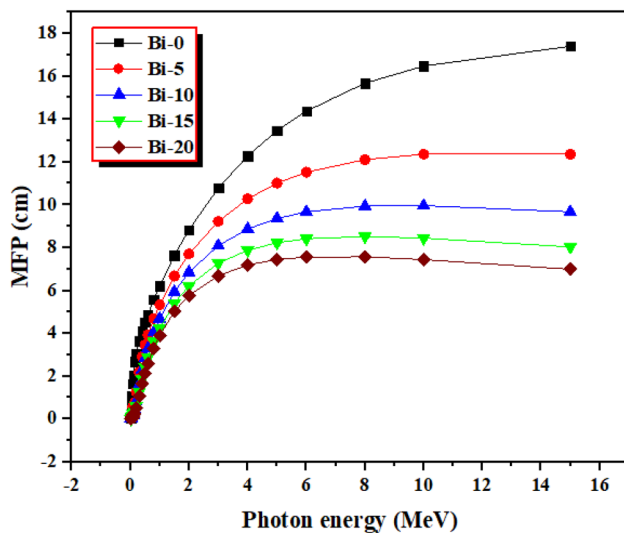


Fig. 11 MFP of Bi0-Bi-20 glasses as a function of photon energy

is observed in Fig. 10 as HVL decreased with increasing Bi content in the glass matrix, increasing its shielding ability against ionizing radiation, especially gamma rays. The trend presented in Fig. 10 can be divided into three energy zones and discussed due to interaction mechanisms discussed later in the above sections. At any definite energy, HVL is seen to take the order that Bi-0 > Bi-5 > Bi-10 > Bi-15 > Bi-20. Furthermore, at 0.015 MeV, HVL decreased from 0.022 cm to 0.003 cm, while at 15 MeV, it decreased from 12.062 cm to 4.841 cm for Bi-0 and Bi-20 glasses.

In a similar way to HVL, MFP, which expressed the distance between two successive interactions between photon and the glass material, is also calculated and plotted in Fig. 11. the same trend as what is obtained in HVL is found, and all results introduced Bi-20 glass sample as a superior candidate for gamma-ray shielding applications.

The transmission factor (%) is used to calculate the number of photons that penetrate the glass thickness and reach the detector. This number depended upon two principal factors, glass thickness, and the incident photon energy. Figure 12a showed the variation of the TF values with the projected photon energy. It is clear that, at low energy, all the projected photon energies were absorbed inside the glass layers due to the PE interaction. The projected photons energy totally absorbed in the PE interaction, and the photon is annihilated inside the material. Thus, there are lower photon numbers that can transmit the shielding material. In this case, Bi-5, Bi-10, Bi-15, and Bi-20 glass samples absorb around 99% of the incident photon in the energy range between 0.015 MeV and 15 MeV. After that, with increasing the photon energy, the PE interaction decreases, and CS starts to be the main interaction in the glass layers. Thus, the number of photons transmitted raised. The average photons absorbed in the energy interval between 0.15 MeV and 1.5 MeV is 43.34%, 51.60%, 57.59%, 62.02%, and 65.16% of the incoming photons for glasses Bi-0, Bi-5, Bi-10, Bi-15, and Bi-20, respectively. Photons with energy higher than 3 MeV possess high energy and high penetration power. Thus. It can penetrate the glass layer with the lowest number of interactions with the material atoms. As a result, the number of absorbed photons inside the glass layers decreased. The average number of photons absorbed in the glass layers is 18.87%, 23.27%, 27.35%, 30.95%, and 33.951% for the fabricated glasses Bi-0, Bi-5, Bi-10, Bi-15, and Bi-20, respectively.

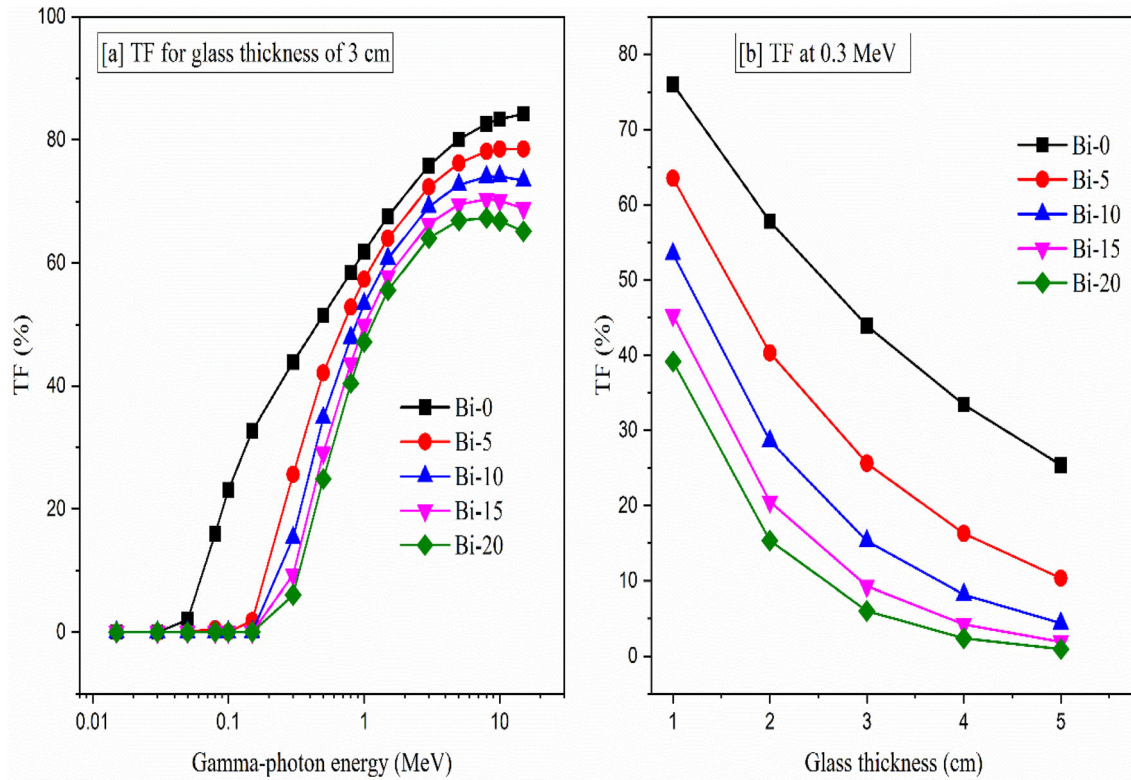


Fig. 12 TF of Bi0-Bi-20 glasses as **a** a function of photon energy at thickness of 3 cm and **b** a function of glass thickness at 0.3 MeV

Figure 12b illustrates the dependence of the TF values on the glass thickness. Increasing the glass thickness leads to occur more interactions between the incident photons and the glass atoms. As a result, a high amount of photon energy is absorbed in the thicker thicknesses. Thus, the number of photons penetrate the thickness decreases. For example, the

TF values for glass Bi-0 at energy 0.3 MeV decreased between 76.02%, 57.79%, 43.93%, 33.40%, and 25.39%. Also, the TF for glass samples Bi-20 decreased between 39.17%, 15.34%, 6.01%, 2.35%, and 0.92% with increasing the glass thickness between 1 cm, 2 cm, 3 cm, 4 cm, and 5 cm, respectively.

Effective atomic number (Z_{eff}) is the parameter that expresses the shielding capacity of material composed of mixture elements, not a single element. It has been calculated based on the MAC values. The effect of chemical composition on the shielding capacity of glasses is more obvious when discussing the Z_{eff} parameter. It is presented in Fig. 13 for all Bi-glasses with respect to photon energy from 0.015 MeV up to 15 MeV. Z_{eff} values increase with photon energy at the beginning of the energy spectrum. After that, the giant hump is noticed at 0.09053 MeV for Bi-5 to Bi-20 without an appearance in Bi-0 due to the K-edge of Bi forming the glass matrix with high molar ratios. After that, at 0.1 MeV < energy range < 1 MeV, Z_{eff} values declined sharply. At MeV > E > 1 MeV, a slight change with photon energy is noticed, and at the highest energy zone, E > 3 MeV, Z_{eff} increased again.

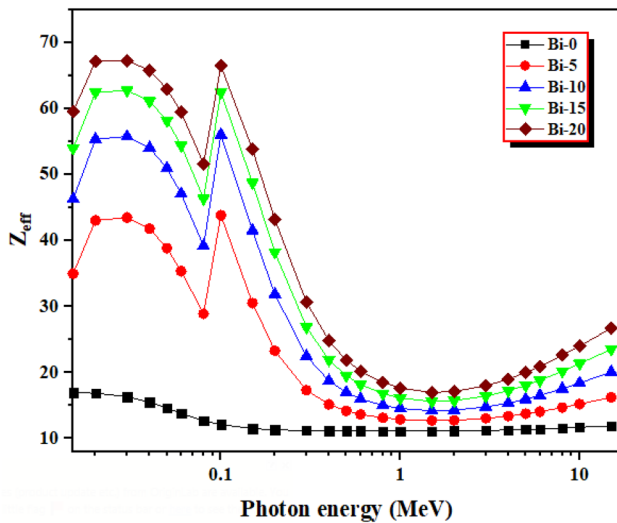


Fig. 13 Z_{eff} of Bi0-Bi-20 glasses as a function of photon energy

This behavior is discussed regarding a photon's three important interaction mechanisms with matter: photoelectric effect, Compton scattering, and pair production. At 0.015 MeV, Z_{eff} values increased from 16.98 to 59.66 while increased from 11.95 to 26.72 at 15 MeV for Bi-0 and Bi-20, respectively.

The equivalent atomic number based mainly on the ratio of $[(\text{MAC})_{\text{CS}}/(\text{MAC})_{\text{total}}]$. Thus, the highest Z_{eq} values were achieved at the mid-energy region, where the CS is the highest compared to the low and high energy regions. The Z_{eq} values reach a maximum around 1 MeV, where the CS is the predominant interaction. At the mentioned energy, Z_{eq} takes values 15.55, 46.87, 55.16, 60.15, and 63.63 for glass samples Bi-0, Bi-5, Bi-10, Bi-15, and Bi-20, respectively. Above 1 MeV, Z_{eq} values began to decrease gently with increasing the photon energy due to the remarkable increase in the PP interaction associated with CS interaction decrease as in Fig. 14.

The exposure and energy absorption buildup factors (EBF and EABF) values were calculated for the Bi-glasses using the Phy-X/PSD software program in the gamma-ray energy interval between 0.015 MeV and 15 MeV. The penetration depth in the unit of mfp was chosen to vary between 0.5 and 40. From the first look at the presented Figures, we can conclude that both EBF and EABF values were increased with raising the Bi_2O_3 incrementation inside the glass samples. This is related to the effective atomic number of the investigated glass where the Z_{eff} increased with increasing the Bi_2O_3 ratio. As the Z number of

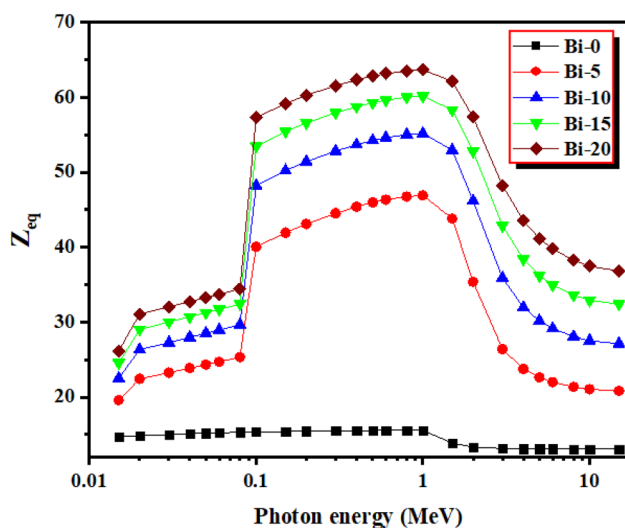


Fig. 14 Z_{eq} of Bi0-Bi-20 glasses as a function of photon energy

the shielding materials increases, photons' accumulation inside the material layer increases, leading to an increase in EBF and EABF values (Figs. 15 and 16).

In addition, the gamma photon energy affected the calculated EBF and EABF values. Both EBF and EABF start small values at low gamma energy due to the PE interaction, which absorbs the photon energy totally. For glasses with Bi_2O_3 concentration > 0 mol%, an increase in EBF and EABF values was detected near 0.1 MeV due to K-edges of Bi as shown in Figs. 15 and 16. Another peak appears near 0.02 MeV for glasses with a higher Bi_2O_3 content ($\text{Bi}_2\text{O}_3 > 10$ mol%). This peak may be due to the X-ray L1 edges of Bi. After that, with increasing the CS interaction in the energy interval starting from $E > 0.15$ MeV, a high accumulation of photons achieved in between the glass layers. This high accumulation is the CS interaction that consumes only a part of the photon energy during the interaction. In the high-energy region where the PP interaction is dominant, a huge increase in EBF and EABF values were achieved.

The third and final parameter is the penetration depth (PD). With increasing the source to detector distance, the photons make more collisions along photons' path length. Thus, the accumulation of photons increases with increasing the penetration depth. So, the calculated values of EBF and EABF increase with increasing the PD values, and a high increase is detected for high PD values (i.e., $\text{PD} > 20$ mfp).

Figure 17 showed the effect of Bi_2O_3 insertion ratio on the fast neutron removal cross-section \sum_{R} ($\text{cm}^2 \text{g}^{-1}$). It is clear from Fig. 17 that the \sum_{R} ($\text{cm}^2 \text{g}^{-1}$) values diminished with the raising the replacement of K_2O by the Bi_2O_3 content. The \sum_{R} take values $0.03248 \text{ cm}^2/\text{g}$, $0.02931 \text{ cm}^2/\text{g}$, $0.02691 \text{ cm}^2/\text{g}$, $0.02504 \text{ cm}^2/\text{g}$, and $0.02355 \text{ cm}^2/\text{g}$ for glass samples Bi-0, Bi-5, Bi-10, Bi-15, and Bi-20 respectively with Bi_2O_3 content 0 mol%, 5 mol%, 10 mol%, 15 mol%, and 20 mol%. This behavior is related to the replacement of K with a highly microscopic cross-section by Bi with a lower microscopic cross-section for the fast neutron.

4 Conclusion

In this work, we present an extensive study of the optical (linear/non-linear). Mechanical properties and gamma photon shielding effectiveness of

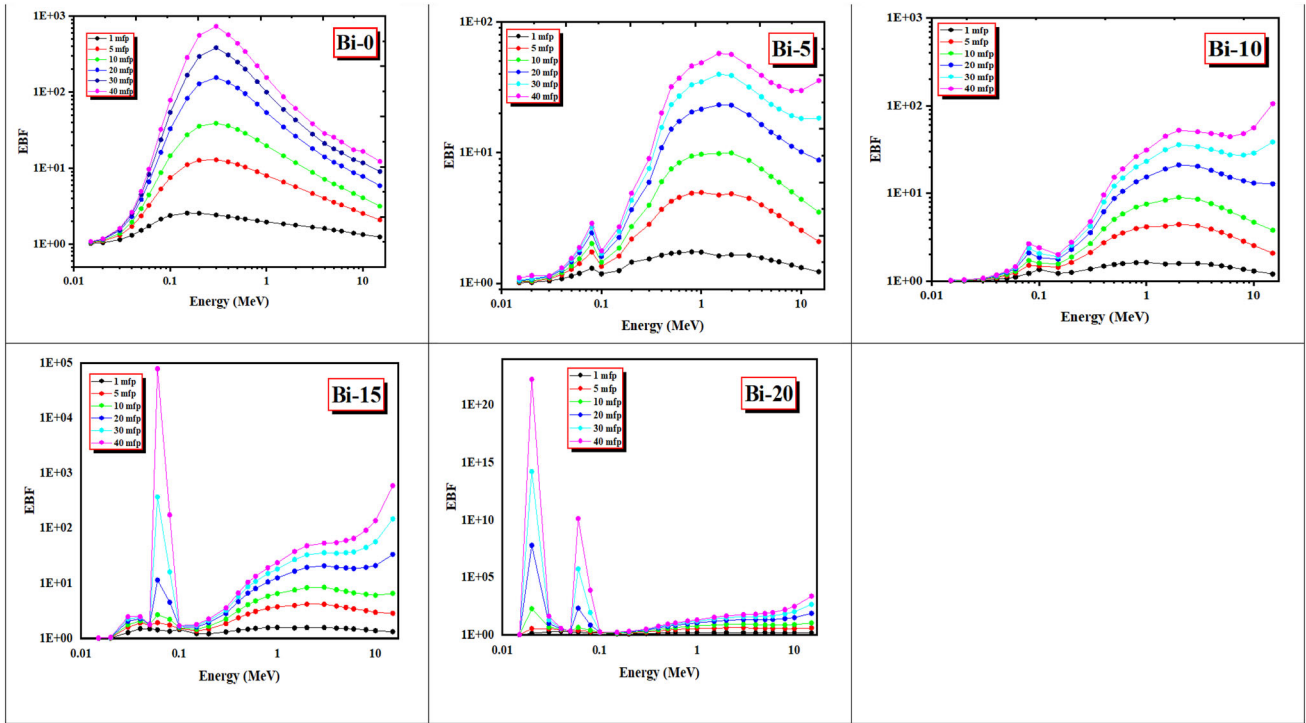


Fig. 15 EBF of the investigated Bi-glasses

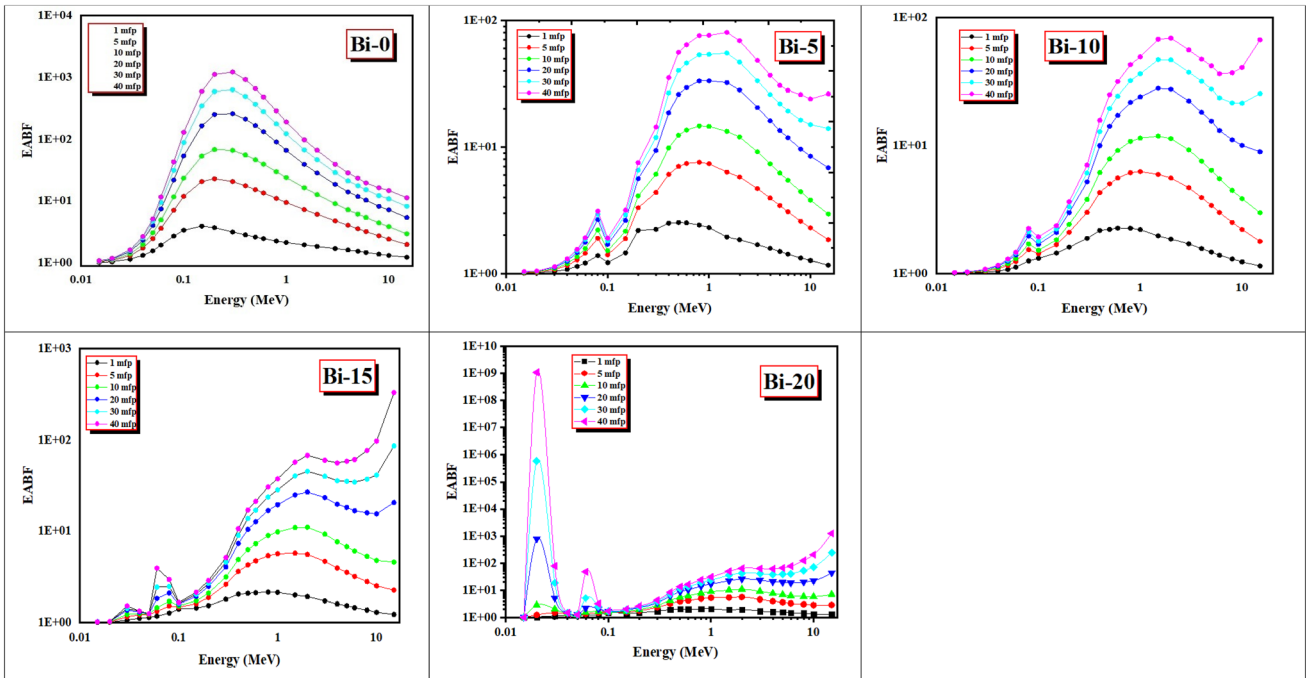


Fig. 16 EABF of the investigated Bi-glasses

potassium titanate biso-phosphate with chemical form $50P_2O_5-30TiO_2-(20-x)K_2O-xBi_2O_3$: $x = 0$ mol%, 5 mol%, 10 mol%, 15 mol%, and 20 mol% encoded as

Bi-0, Bi-5, Bi-10, Bi-15, and Bi-20. Results revealed that:

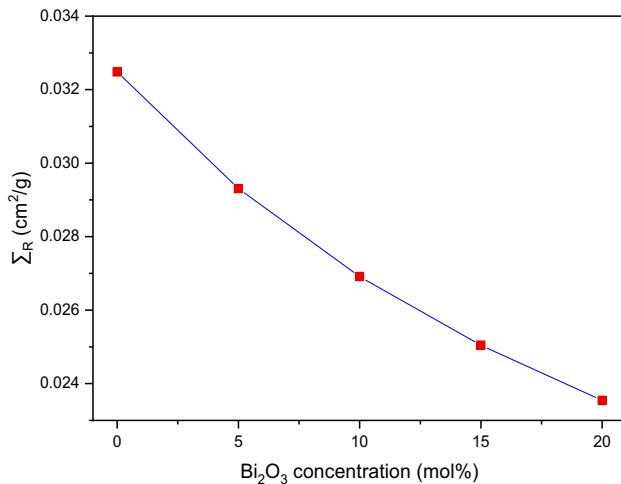


Fig. 17 Z_{eq} of Bi0-Bi-20 glasses as a function of photon energy

1. The linear refractive index ($n^{optical}$) was increased from 2.41 for Bi-0 (free from Bi^{3+} ions) glass sample to 2.52 for Bi-20 (rich with Bi^{3+} ions) glass sample.
2. The (R^{molar}) and (α^{molar}) were enhanced with the addition of Bi^{3+} ions content due to the increase of the number of nonbridging oxygen (NBO) atoms in the glass structure.
3. Value of (χ^*) was reduced from 0.792 to 0.688, while ($\chi^{(1)}$) was increased from 0.383 to 0.428 with the increase of Bi^{3+} ions from 0 to 20 mol%.
4. Both of the $\chi^{(3)}$ and $n_2^{optical}$ were enhanced with the addition of Bi^{3+} ions in the investigated glasses.
5. Bond compression bulk elastic (K_{B-C}) modulus was found to decrease from 72.737 GPa for Bi-0 to 69.266 GPa for Bi-20 glasses, while Poisson's ratio (σ_{B-C}) for Bi-glasses was increased from 0.251 to 0.256.
6. According to Makishima-Mackenzie (M-M) model, values of (E_{M-M}) were decreased from 56.296 to 55.789 GPa, (K_{M-M}) from 39.370 to 36.775 GPa, and slight increases in the (S_{M-M}) from 22.310 to 22.366 (GPa). Poisson's ratio (σ_{M-M}) for Bi-glasses was decreased from 0.261 to 0.247.
7. In terms of MAC and LAC the glasses take the order that $(Bi-0)^{MAC,LAC} < (Bi-5)^{MAC,LAC} < (Bi-10)^{MAC,LAC} < (Bi-15)^{MAC,LAC} < (Bi-20)^{MAC,LAC}$.
8. In terms of HVL, at 0.015 MeV, HVL decreased from 0.022 to 0.003 cm, while at 15 MeV, it

decreased from 12.062 to 4.841 cm for Bi-0 and Bi-20 glasses.

9. In terms of transmission factor (TF), the average photons absorbed in the energy interval between 0.15 MeV and 1.5 MeV is 43.34%, 51.60%, 57.59%, 62.02%, and 65.16% of the incoming photons for glasses Bi-0, Bi-5, Bi-10, Bi-15, and Bi-20, respectively.
10. The calculated values of EBF and EABF increase with increasing the PD values, and a high increase is detected for high PD values (i.e., $PD > 20$ mfp).
11. The \sum_R take values 0.03248 cm²/g, 0.02931 cm²/g, 0.02691 cm²/g, 0.02504 cm²/g, and 0.02355 cm²/g for glass samples Bi-0, Bi-5, Bi-10, Bi-15, and Bi-20, respectively.

Generally, the results in this work confirm that studied Bi-glasses can be used as a candidate for several optical application such as optoelectronic devices, optical fibers, and optical waveguides. Moreover, Bi-glasses can be considered as superior candidate for gamma-ray shielding applications.

Acknowledgements

Taif University Researchers Supporting Project number (TURSP-2020/84), Taif University, Taif, Saudi Arabia.

References

1. R.K. Brow, D.R. Tallant, Structural design of sealing glasses. *J Non Cryst Solids* **222**, 396–406 (1997)
2. I. Jlassi, N. Sdiri, H. Elhouichet, Electrical conductivity and dielectric properties of MgO doped lithium phosphate glasses. *J Non Cryst. Solids* **466–467**, 45–51 (2017)
3. P.S. Rao, C. Rajyasree, A.R. Babu, P.M.V. Teja, D.K. Rao, Effect of Bi_2O_3 proportion on physical, structural and electrical properties of zinc bismuth phosphate glasses. *J. Non Cryst. Solids* **357**, 3585–3591 (2011)
4. M.S. Shams, Y.S. Rammah, F.I. El-Agawany, R.A. Elsad, Synthesis, structure, physical, dielectric characteristics, and gamma-ray shielding competences of novel $P_2O_5-Li_2O-ZnO-CdO$ glasses. *J Mater Sci: Mater Electron* **32**, 1877–1887 (2021)
5. P.P. Proulx, G. Cormier, J.A. Capobianco, B. Champagnon, M. Bettinelli, Raman and low frequency Raman spectroscopy

- of lead, zinc and barium metaphosphate glasses doped with Eu^{3+} ions. *J. Phys. Condens Matter* **6**, 275–283 (1994)
6. H. Es-soufi, H. Bih, L. Bih, M. Azrou, B. Manoun, P. Lazor, Structure and some physical properties of the sodium ion conducting glasses inside the $\text{Na}_2\text{O-Na}_2\text{WO}_4\text{-TiO}_2\text{-P}_2\text{O}_5$ system. *J Appl Surfaces Interfaces* **4**(2018), 1–3 (2018)
 7. M. Laourayed, M. El. Moudane, A. Guenbour et al., Glass-forming region, electrical and structural properties of $\text{BiPO}_4\text{-NbOPO}_4\text{-P}_2\text{O}_5$ ($\text{Bi}_2\text{O}_3\text{-Nb}_2\text{O}_5\text{-P}_2\text{O}_5$) glasses. *J Mater.* **8**, 2932–2939 (2017)
 8. P.Y. Shih, Thermal, chemical and structural characteristics of erbium-doped sodium phosphate glasses. *Mater Chem Phys* **84**, 151–156 (2004)
 9. S. Hoseinzadeh, R. Ghasemiasl, A. Bahari, A.H. Ramezani, n-type WO_3 semiconductor as a cathode electrochromic material for ECD devices. *J Mater Sci: Mater Electron* **28**, 14446–14452 (2017). <https://doi.org/10.1007/s10854-017-7306-7>
 10. S. Hoseinzadeh, R. Ghasemiasl, A. Bahari, A.H. Ramezani, The injection of Ag nanoparticles on surface of WO_3 thin film: enhanced electrochromic coloration efficiency and switching response. *J Mater Sci: Mater Electron* **28**, 14855–14863 (2017). <https://doi.org/10.1007/s10854-017-7357-917>
 11. S. Hoseinzadeh, R. Ghasemiasl, A. Bahari, A.H. Ramezani, Effect of post-annealing on the electrochromic properties of layer-by-layer arrangement $\text{FTO-WO}_3\text{-Ag-WO}_3\text{-Ag}$. *Journal of Elec Materi* **47**, 3552–3559 (2018). <https://doi.org/10.1007/s11664-018-6199-4>
 12. A.H. Ramezani, S. Hoseinzadeh, Zh. Ebrahiminejad, M.R. Hantehzadeh, M. Shafiee, The study of mechanical and statistical properties of nitrogen ion-implanted Tantalum bulk. *Optik* **225**(2021), 165628 (2021)
 13. A.H. Ramezani, A. Hoseinzadeh, Zh. Ebrahiminejad, Z. Statistical and fractal analysis of nitrogen ion implanted tantalum thin films. *Appl. Phys. A* **126**, 481 (2020). <https://doi.org/10.1007/s00339-020-03671-7>
 14. A.H. Ramezani, S. Hoseinzadeh, Z.H. Ebrahiminejad, S.F. Masoudi, A. Hashemizadeh, Spin-polarized electron transfer in multilayers with different types of rough interfaces. *J Supercond. Nov. Magn.* **33**, 1513–1519 (2020). <https://doi.org/10.1007/s10948-019-05335-x>
 15. A. Shaim, M. Et-Tabirou, L. Montagne et al., Molar volume, thermal properties and dc conductivity of $\text{Na}_2\text{O-Bi}_2\text{O}_3\text{-TiO}_2\text{-P}_2\text{O}_5$ glasses. *Phys. Chem. Glas.* **44**, 26–29 (2003)
 16. M. Elmoudan, M. Belkhouaja, M. Et-Tabirou, M. Taibi, Glass transition (T_g) and dielectric constant (ϵ_r) of $\text{Li}_3\text{PO}_4\text{-Pb}_3(\text{-PO}_4)_2\text{-BiPO}_4(\text{Li}_2\text{O-PbO-Bi}_2\text{O}_3\text{-P}_2\text{O})$ glasses. *Phase Transitions: A Multinatl J.* **76**, 645–652 (2003)
 17. Ch.S. Rao, K. Seshulatha, Y.S. Gurupria, P. Sagar, M. VijayKumar, S.S. Vali, D. Ramanjaneyulu, S. Kotireddy, Optical properties of $\text{Na}_2\text{SO}_4\text{-B}_2\text{O}_3\text{-P}_2\text{O}_5$ glasses doped with TiO_2 . *Mater Today Proc.* **5**, 26217–26222 (2018)
 18. L. Baia, R. Stefan, W. Kiefer, J. Popp, S. Simon, Structural investigations of copper doped $\text{B}_2\text{O}_3\text{-Bi}_2\text{O}_3$ glasses with high bismuth oxide content. *J Non Cryst Solids* **303**, 379–386 (2002)
 19. M.I. Sayyed, I.A. El-Mesady, A.S. Abouhaswa, A. Askin, Y.S. Rammah, Comprehensive study on the structural, optical, physical and gamma photon shielding features of $\text{B}_2\text{O}_3\text{-Bi}_2\text{O}_3\text{-PbO-TiO}_2$ glasses using WinXCOM and Geant4 code. *J Mol Struct* **1197**, 656–665 (2019)
 20. H.A. ElBatal, E.M.A. Khalil, Y.M. Hamdy, In vitro behavior of bioactive phosphate glass-ceramics from the system $\text{P}_2\text{O}_5\text{-Na}_2\text{O-CaO}$ containing titania. *Ceram Int.* **35**, 1195–1204 (2009)
 21. E. Haily, L. Bih, A. El. Bouari, A. Lahmar, M. El. Marssi, B. Manoun, Structural, optical, and dielectric properties of $\text{Bi}_2\text{O}_3\text{-K}_2\text{O-TiO}_2\text{-P}_2\text{O}_5$ glasses and related glass-ceramics. *Phase Transition* **93**, 1030–1047 (2020)
 22. M. Monisha, N. Mazumder, G. Lakshminarayana, S. Mandal, S.D. Kamath, Energy transfer and luminescence study of Dy^{3+} doped zinc- aluminoborosilicate glasses for white light emission. *Ceram. Int.* **47**(2021), 598–610 (2021)
 23. M.K. Halimah, M.F. Faznny, M.N. Azlan, H.A.A. Sidek, Optical basicity and electronic polarizability of zinc borotellurite glass doped La^{3+} ions. *Results Phys.* **7**, 581–589 (2017)
 24. S.A. Umar, M.K. Halimah, K.T. Chan, A.A. Latif, Polarizability, optical basicity and electric susceptibility of Er^{3+} doped silicate borotellurite glasses. *J. Non-Cryst. Solids* **471**, 101–109 (2017)
 25. J.A. Duffy, *Bonding, Energy Level and Bonds in Inorganic Solids* (Longman, England, 1990)
 26. M.S. Dresselhaus, Solid state physics part II: optical properties of solids, *Proceedings Int. Sch. Phys.* (1966) 198.
 27. H. Ticha, L. Tichy, Semiempirical relation between non-linear susceptibility (refractive index), linear refractive index and optical gap and its application to amorphous chalcogenides. *J. Optoelectron. Adv. Mater.* **4**, 381–386 (2002)
 28. I.O. Olarinoye, F.I. El-Agawany, A. El-Adawy, Y.S. El-Sayed Yousef, Y.S. Rammah, Mechanical features, alpha particles, photon, proton, and neutron interaction parameters of $\text{TeO}_2\text{-V}_2\text{O}_3\text{-MoO}_3$ semiconductor glasses. *Ceram Int* (2020). <https://doi.org/10.1016/j.ceramint.2020.06.093>
 29. Y.S. Rammah, I.O. Olarinoye, F.I. El-Agawany, A. El-Adawy, A. Gamal, El Sayed Yousef. Elastic moduli, photon, neutron, and proton shielding parameters of tellurite 19 bismo-vanadate ($\text{TeO}_2\text{-V}_2\text{O}_5\text{-Bi}_2\text{O}_3$) semiconductor glasses. *Int Ceram.* <https://doi.org/10.1016/j.ceramint.2020.07.014>

30. N. Elkshokhany, E. Syala, E. Yousef, Concentration dependence of the elastic moduli, thermal properties, and non-isothermal kinetic parameters of Yb^{3+} doped multicomponent tellurite glass system. *Results Phys.* **16**, 102876 (2020)
31. X-5 Monte Carlo Team, MCNP-A General Monte Carlo N-Particle Transport Code, Version 5, Los Alamos Controlled Publication. LA-CP-03-0245, 2003.
32. K.M. Kaky, M.I. Sayyed, M.H.A. Mhareb, A.H. Abdalsalam, K.A. Mahmoud, S.O. Baki, M.A. Mahdi, Physical, structural, optical and gamma radiation attenuation properties of germanate-tellurite glasses for shielding applications. *Journal of Non-Crystalline Solids* **545**, 120250 (2020). <https://doi.org/10.1016/j.jnoncrsol.2020.120250>
33. M.I. Sayyed, A.A. Ali, M.H.A. Mhareb, K.A. Mahmoud, K.M. Kaky, S.O. Baki, M.A. Mahdi, Novel tellurite glass $(60-x)\text{TeO}_2-10\text{GeO}_2-20\text{ZnO}-10\text{BaO}-x\text{Bi}_2\text{O}_3$ for radiation shielding. *J. Alloy. Compd.* **844**, 155668 (2020). <https://doi.org/10.1016/j.jallcom.2020.155668>
34. S.A.M. Issa, T.A. Hamdalla, A.A.A. Darwish, Effect of ErCl_3 in gamma and neutron parameters for different concentration of $\text{ErCl}_3\text{-SiO}_2$ (EDFA) for the signal protection from nuclear radiation. *J. Alloys Compd.* **698**, 234–240 (2017)
35. D.K. Gaikwad, S.S. Obaid, M.I. Sayyed, R.R. Bhosale, V.V. Awasarmol, A. Kumar, M.D. Shirsat, P.P. Pawar, Comparative study of gamma ray shielding competence of $\text{WO}_3\text{-TeO}_2\text{-PbO}$ glass system to different glasses and concretes. *Mater Chem. Phys.* **213**, 508–517 (2018)
36. Y.S. Rammah, F.I. El-Agawany, K.A. Mahmoud, R. El-Mallawany, Erkan Ilik, Gokhan Kilic, FTIR, UV–Vis–NIR spectroscopy, and gamma rays shielding competence of novel ZnO-doped vanadium borophosphate glasses. *J. Mater. Sci.: Mater. Electron.* (2020). <https://doi.org/10.1007/s10854-020-03440-5>
37. V.P. Singh, H.O. Tekin, N.M. Badiger, T. Manici, E.E. Altunsoy, Effect of heat treatment on radiation shielding properties of concretes. *J. Radiat. Protect. Res* **43**(1), 20–28 (2018). <https://doi.org/10.14407/jrpr.2018.43.1.20.20>
38. Y.S. Rammah, Influence of Ag_2O insertion on alpha, proton and γ -rays safety features of $\text{TeO}_2\text{-ZnO.Na}_2\text{O}$ glasses: Potential use for nuclear medicine applications. *Ceram. Int.* (2020). <https://doi.org/10.1016/j.ceramint.2020.04.136>
39. C. Bootjomchai, J. Laopaiboon, C. Yenchai, R. Laopaiboon, Gamma-ray shielding and structural properties of barium-bismuth-borosilicate glasses. *Radiat. Phys. Chem.* **81**, 785–790 (2012). <https://doi.org/10.1016/j.radphyschem.2012.01.049>
40. A.A.A. Darwish, S.A.M. Issa, M.M. El-Nahass, Effect of gamma irradiation on structural, electrical and optical properties of nanostructure thin films of nickel phthalocyanine. *Synth. Methods* **215**, 200–206 (2016). <https://doi.org/10.1016/j.synthmet.2016.03.002>
41. B.O. Elbashir, M.G. Dong, M.I. Sayyed, S.A.M. Issa, K.A. Matori, M.H.M. Zaid, Comparison of Monte Carlo simulation of gamma-ray attenuation coefficients of amino acids with XCOM program and experimental data. *Results Phys.* **9**, 6–11 (2018). <https://doi.org/10.1016/j.rinp.2018.01.075>
42. S.A.M. Issa, Y.B. Saddeek, H.O. Tekin, M.I. Sayyed, K. Saber Shaaban, Investigations of radiation shielding using Monte Carlo method and elastic properties of $\text{PbO-SiO}_2\text{-B}_2\text{O}_3\text{-Na}_2\text{O}$ glasses. *Curr. Appl. Phys.* **18**, 717–727 (2018)
43. Y.S. Rammah, Evaluation of radiation shielding ability of boro-tellurite glasses: $\text{TeO}_2\text{-B}_2\text{O}_3\text{-SrCl}_2\text{-LiF-Bi}_2\text{O}_3$. *Appl. Phys. A* **125**, 857 (2019)
44. F.I. El-Agawany, E. Kavaz, U. Periřanođlu, M. Al-Buriah, Y.S. Rammah, Sm_2O_3 effects on mass stopping power/projected range and nuclear shielding characteristics of $\text{TeO}_2\text{-ZnO}$ glass systems. *Appl. Phys. A* **125**, 838 (2019)
45. M. S. Al-Buriah, H. O. Tekin, E. Kavaz, B.T. Tonguc, Y. S. Rammah, New transparent rare earth glasses for radiation protection applications. *Appl. Phys. A* **125**, 866 (2019)
46. M.S. Al-Buriah, Y.S. Rammah, Electronic polarizability, dielectric, and gamma-ray shielding properties of some tellurite-based glasses. *Appl. Phys. A* **125**, 678 (2019)
47. E. řakar, Ö.F. Özpolat, B. Alım, M.I. Sayyed, M. Kurudirek, Phy-X/PSD: Development of a user friendly online software for calculation of parameters relevant to radiation shielding and dosimetry. *Radiat. Phys. Chem.* **166**, 108496 (2020)

Publisher's Note Springer Nature remains neutral with regard to jurisdictional claims in published maps and institutional affiliations.